PHYSICAL REVIEW D **91,** 114023 (2015)

B meson semi-inclusive decay to spin-triplet D-wave charmonium in NRQCD

Sheng-Jing Sang,[1] Jin-Zhao Li,[1] Ce Meng,[1] and Kuang-Ta Chao[1,2,3]

[1]*School of Physics and State Key Laboratory of Nuclear Physics and Technology, Peking University, Beijing 100871, China*

[2]*Center for High Energy Physics, Peking University, Beijing 100871, China*

[3]*Collaborative Innovation Center of Quantum Matter, Beijing 100871, China*

(Received 7 April 2015; published 18 June 2015)

We study the B meson semi-inclusive decays into spin-triplet D-wave chamonium states $\psi_J (J = 1, 2, 3)$ based on the nonrelativistic QCD factorization formula at next-to-leading order in α_s and leading order in v (the relative velocity of charm quark and antiquark in charmonium). The finite short-distance coefficients for ${}^3D_J^{[1]}$ channels are obtained for the first time. The long-distance matrix elements are estimated with the help of potential model and QCD evolution equations. The branching ratios $\mathrm{Br}(B \to \psi_1 X)$ and $\mathrm{Br}(B \to \psi_2 X)$ are, respectively, predicted to be about 6×10^{-4} and 2×10^{-3}, with about 50% relative errors mainly coming from the uncertainties of long-distance matrix elements. The branching ratio $\mathrm{Br}(B \to \psi_3 X)$ can be very small due to a possible cancellation between the ${}^3S_1^{[8]}$ and ${}^3P_2^{[8]}$ channels. As an optimistic estimate, we may use the ${}^3S_1^{[8]}$ channel alone to set up the upper limit for $\mathrm{Br}(B \to \psi_3 X)$, which is about 4×10^{-4} and may be used in searching for the missing state ψ_3.

DOI: 10.1103/PhysRevD.91.114023 PACS numbers: 12.38.Bx, 13.20.He, 14.40.Pq

I. INTRODUCTION

The decays of the B meson into charmonium states are important processes to study the Cabibbo-Kobayashi-Maskawa matrix and CP violation. In recent years these processes have also been used to search for the missing higher charmonium states and to study the properties of chamoniumlike states, the so-called XYZ mesons (for recent reviews see Refs. [1–3] and references therein). These studies are important for understanding the underlying dynamics of strong interactions. In 2013, Belle Collaboration found evidence for a new narrow resonance $X(3823)$ in the mass spectrum of $\chi_{c1}\gamma$ in the $B^\pm \to \chi_{c1}\gamma K^\pm$ decay with branching ratio product [4]

$$\mathrm{Br}(B^\pm \to X(3823)K^\pm) \cdot \mathrm{Br}(X(3823) \to \chi_{c1}\gamma) = (9.7 \pm 2.8 \pm 1.1) \times 10^{-6}. \quad (1)$$

The mass of $X(3823)$ and the ratio $\mathrm{Br}(X \to \chi_{c2}\gamma)/\mathrm{Br}(X \to \chi_{c1}\gamma) < 0.41$ at 90% C.L. [4] are all consistent with those expected for the $\psi_2(1^3D_2)$ $c\bar{c}$ state. This assignment is also consistent with the observation that no peak around 3823 GeV is seen in the $D\bar{D}$ spectrum in the $B \to D\bar{D}K$ decay [5], as ψ_2 with the unnatural quantum number $J^P = 2^-$ cannot decay into $D\bar{D}$. Moreover, the partial decay width to light hadrons is estimated to be $\Gamma(\psi_2 \to \mathrm{LH}) \sim 50$ keV [6], while potential model calculations indicate that $\Gamma(\psi_2 \to \gamma\chi_{c1}) = (208\text{–}342)$ keV and $\Gamma(\psi_2 \to \gamma\chi_{c2}) = (55\text{–}70)$ keV [7]. Thus, one may expect that the decay mode $\chi_{c1}\gamma$ is the dominant one for ψ_2 and the corresponding branching ratio is no less than 50% [6]. Therefore, with the assumption that $X(3823) = \psi_2$, Eq. (1) will roughly imply that

$$1 \times 10^{-5} < \mathrm{Br}(B \to \psi_2 K) < 2 \times 10^{-5}, \quad (2)$$

which is smaller than the production rate of J/ψ in the similar B decay process [8] by one order of magnitude or more. This is quite natural since the production rate of the D-wave state should be suppressed by a factor of $v^4 \sim 0.1$ relative to that of the S-wave state in the factorization hypothesis, where v denotes the relative velocity of the charm quark pair in the rest frame of charmonium.

On the other hand, as for $\psi(3770)$, which is usually expected to be predominantly the $\psi_1(1^3D_1)$ state with a small admixture of the $\psi(2^3S_1)$ component (S-D mixing), it has a surprisingly large production rate in the B decay [8]:

$$\mathrm{Br}(B^+ \to \psi(3770)K^+) = (4.9 \pm 1.3) \times 10^{-4}, \quad (3)$$

which is comparable to that of $\psi(3686) \approx \psi(2^3S_1)$. Even if one take into account the S-D mixing effects, the large production rate of $\psi(3770)$ can hardly be explained unless the contributions from soft gluon interactions are numerically large [9]. However, the soft gluon interactions make the factorization break down, therefore, the calculations are model dependent.

While the calculations for exclusive B decays into charmonium are complicated and often suffer from large uncertainties due to factorization violation effects, especially for the P-wave [10] and D-wave [9] charmonium final states, those for inclusive B decays can be well handled within the framework of nonrelativistic QCD (NRQCD) factorization [11]. Moreover, the inclusive production rates of chamonium in B decays can constrain the exclusive ones quite strictly. The fraction of exclusive two-body (charmonium H plus K meson) production rate in B decay relative to the inclusive one

$$R_2(H) = \frac{\mathrm{Br}(B \to HK)}{\mathrm{Br}(B \to H + \mathrm{anything})} \tag{4}$$

is about $1/10$ for $H = J/\psi, \psi(3686), \chi_{c1}$, and even smaller than $1/100$ for $H = \chi_{c2}$ [8]. Therefore, it is interesting to study the production rate of the spin-triplet states $\psi_J(1^3D_J)(\mathrm{J} = 1, 2, 3)$ in the inclusive B decays on a relative reliable theoretical basis, and also to see whether the results can be consistent with the large exclusive production rate in (3).

On the other hand, the direct measurements on the decays $B \to \psi_J X$ are themselves interesting and important for testing the NRQCD factorization approach and for determining the long-distance matrix elements related to ψ_J production. In particular, since the ψ_3 state is still missing, it is very useful to see whether the estimated production rate of ψ_3 can be large enough to search for it in the B decay processes.

The inclusive production of ψ_J in B decays has been studied at the leading order (LO) in α_s [12,13] based on NRQCD factorization. However, the next-to-leading order (NLO) corrections in α_s have proved to be very important for similar inclusive production processes of S-/P-wave [14] and spin-singlet D-wave [15] charmonium states. Thus, in this paper, we will extend the NLO calculations in Refs. [14,15] to the ψ_J case. In Sec. II, we set up the general notations and provide the LO results. The NLO calculations are given in Sec. III, including how to get the ultraviolet (UV) and infrared (IR) finite short-distance coefficients, and how to estimate the long-distance matrix elements. In Sec. IV, numerical results are given and discussed, and a short summary is finally given in Sec. V.

II. GENERAL NOTATION AND LO RESULTS

The weak effective Hamiltonian relevant here has the form

$$H_{\mathrm{eff}} = \frac{G_F}{\sqrt{2}} \sum_{q=s,d} \left\{ V_{cb}^* V_{cq} \left[\frac{1}{3} C_{[1]}(\mu) \mathcal{O}_1(\mu) + C_{[8]}(\mu) \mathcal{O}_8(\mu) \right] - V_{tb}^* V_{tq} \sum_{i=3}^{6} C_i(\mu) \mathcal{O}_i(\mu) \right\}, \tag{5}$$

where the "current-current" operators are given by

$$\begin{aligned} \mathcal{O}_1 &= [\bar{c}\gamma_\mu(1-\gamma_5)c][\bar{b}\gamma^\mu(1-\gamma_5)q], \\ \mathcal{O}_8 &= [\bar{c}T^a\gamma_\mu(1-\gamma_5)c][\bar{b}T^a\gamma^\mu(1-\gamma_5)q], \end{aligned} \tag{6}$$

and the $\mathcal{O}_{3\text{–}6}$ denote the QCD penguin operators. The renormalization group improved NLO results for the Wilson coefficients $C_{[1]}(\mu)$ and $C_{[8]}(\mu)$ (where [1]/[8] denotes the color singlet/octet representation of the outgoing $c\bar{c}$ pair) and $C_{3\text{–}6}(\mu)$ can be found in Ref. [16]. Numerically, $C_{3\text{–}6}(\mu)$ are extremely small. And, compared with $C_{[8]}(\mu)$, $C_{[1]}(\mu)$ is relative small and sensitive to the renormalization scale μ. At the scale $\mu \sim m_b$, the ratio $C_{[8]}^2/C_{[1]}^2 \sim 15$, which can explain why the color-octet (CO) production mechanism in NRQCD factorization is of particular important in the inclusive production of charmonium in B decays [12–15]. This fact can also roughly account for the smallness of the ratio in (4) since the CO $c\bar{c}$ pair needs to emit soft gluons to evolve to the physical charmonium state, and the reabsorption of the soft gluons by the spectator quark to form a single K meson tends to be an affair with small probability.

With the NRQCD factorization formula [11], the semi-inclusive decay width of the B meson into charmonium H can be expressed as

$$\begin{aligned} \Gamma(B \to H + X) &= \sum_n \Gamma[n] \\ &= \sum_n C(b \to c\bar{c}[n] + x)\langle \mathcal{O}^H[n] \rangle, \end{aligned} \tag{7}$$

which is valid up to power corrections of order $\Lambda_{\mathrm{QCD}}/m_{b,c}$. Here, $C(b \to c\bar{c}[n] + x) \equiv C[n]$ denotes the short-distance coefficient corresponding to the production of the $c\bar{c}$ pair in configuration n, which can be calculated perturbatively in α_s, and the long-distance matrix elements (LDMEs) $\langle \mathcal{O}^H[n] \rangle$ describe the probabilities for the evolution of $c\bar{c}[n]$ to charmonium H, and thus are insensitive to the hard processes and are universal parameters. Moreover, the LDMEs can be arranged as a series in the power expansion of v^2. For the production of $\psi_J(J = 1, 2, 3)$ at LO in v^2, one only needs to calculate the short-distance coefficients (SDCs) for

$$n \in \{ {}^3S_1^{[1]}, {}^3S_1^{[8]}, {}^3P_{J'=0,1,2}^{[8]}, {}^3D_J^{[1]} \}, \tag{8}$$

where n is classified by ${}^{2S+1}L_J^{[C]}$, and, respectively, S, L and J denote the spin, the orbital angular momentum and the total angular momentum, and $C = 1, 8$ refer to color-singlet (CS) and CO configurations. The relevant operators $\mathcal{O}^H[n]$ are listed in Appendix A.

Up to the NLO in α_s by taking advantage of $|V_{cs}|^2 + |V_{cd}|^2 \approx 1$, it is convenient to express the partial decay rates $\Gamma[n]$ in (7) as [14]

$$\Gamma[n] = \Gamma_0 \left[C_{[1,8]}^2 f[n](\eta)(1 + \delta_P[n]) + \frac{\alpha_s(\mu)}{4\pi} (C_{[1]}^2 g_1[n](\eta) + 2C_{[1]}C_{[8]} g_2(\eta) + C_{[8]}^2 g_3[n](\eta)) \right] \frac{\langle \mathcal{O}^H[n] \rangle}{m_c^{d-3}}, \tag{9}$$

where

$$\Gamma_0 = \frac{G_F^2 |V_{bc}|^2 m_b^3}{216\pi(2m_c)}, \tag{10}$$

$\eta = 4m_c^2/m_b^2$, $\delta_P[n]$ is the penguin correction factor and d denotes the dimension of the NRQCD operator. Then the decay width is simplified to the calculations of the reduced SDC f's and g's in Eq. (9) for the relevant configurations in (8).

Because of the $(V-A)$ structure of the current-current operators in (6), only for $n = {}^3S_1^{[1]}, {}^3S_1^{[8]}, {}^3P_1^{[8]}, {}^3D_1^{[1]}$ in (8), the LO coefficient f's are nonzero, and they are

$$\begin{aligned} f[{}^3S_1^{[1]}](\eta) &= (1-\eta)^2(1+2\eta), \\ f[{}^3S_1^{[8]}](\eta) &= \frac{3}{2}(1-\eta)^2(1+2\eta), \\ f[{}^3P_1^{[8]}](\eta) &= 3(1-\eta)^2(1+2\eta), \\ f[{}^3D_1^{[1]}](\eta) &= \frac{5}{12}(1-\eta)^2(1+2\eta), \end{aligned} \tag{11}$$

which are consistent with the previous calculations [12–14].

Since the Wilson coefficients of QCD penguin operators $C_{3\text{–}6}$ are much smaller than $C_{[1]}$ and $C_{[8]}$, the double penguin contributions are suppressed. One only needs to calculate the interference between QCD penguin operators $\mathcal{O}_{3\text{–}6}$ and the current-current operators. It is sufficient to evaluate the penguin contributions at the LO in α_s with Wilson coefficients $C_3(m_b)=0.010, C_4(m_b)=-0.024, C_5(m_b)=0.007, C_6(m_b)=-0.028$ together with $C_{[1]}^{\mathrm{LO}}(m_b) = 0.42$ and $C_{[8]}^{\mathrm{LO}}(m_b) = 2.19$ [14], which give nonzero correction factors

$$\delta_P[{}^3S_1^{[1]}] = \delta_P[{}^3D_1^{[1]}] = 2\frac{3(C_3+C_5)+C_4+C_6}{C_{[1]}} \approx -0.005, \tag{12a}$$

$$\delta_P[{}^3S_1^{[8]}] = 4\frac{C_4+C_6}{C_{[8]}} \approx -0.095, \tag{12b}$$

$$\delta_P[{}^3P_1^{[8]}] = 4\frac{C_4-C_6}{C_{[8]}} \approx 0.007. \tag{12c}$$

III. NLO RESULTS AND EVOLUTIONS OF LDMES

In this section we will present some details in the analytical NLO calculations, especially for the ${}^3D_J^{[1]}$ Fock state, since the SDCs for other Fock states (${}^3S_1^{[1]}, {}^3S_1^{[8]}, {}^3P_{J'}^{[8]}$) were calculated in Ref. [14]. And then, we will estimate the LDMEs by using the evolution equations in NRQCD.

A. SDCs at NLO in α_s

The relevant Feynman diagrams for the NLO QCD corrections are all shown in Fig. 1, where $(s_{1\text{–}4}), (v_{1\text{–}6})$ and $(r_{1\text{–}4})$ are the self-energy, vertex correction and real correction diagrams, respectively. The four-fermion operator inserted in these diagrams (denoted by the two dots in Fig. 1) is $\mathcal{O}_1$ or $\mathcal{O}_8$ in (6). In calculations of these diagrams, one faces both the UV and the IR divergence. In the following, we will summarize how to treat these divergences and how to get finite short-distance coefficients, and we will refer more details of the calculations to Refs. [14] and [15].

For the UV part, the Ward identity guarantees that by summing up vertex correction diagrams (v_3), (v_6) and the four self-energy diagrams (s_1) to (s_4), we can get an UV finite amplitude. The UV divergences in summing up diagrams (v_1), (v_2) and (v_4), (v_5) are just the same as those appearing in the operator renormalization of $\mathcal{O}_1$ or $\mathcal{O}_8$. Therefore, they can be canceled by introducing counterterms in the weak Hamiltonian in (5). This procedure will introduce the renormalization scale μ dependence to the hadronic matrix element of $\mathcal{O}_{1/8}$, which in principle should be canceled by that of $C_{[1]/[8]}$ up to higher order in α_s.

It needs to be stressed that we use two schemes to treat γ_5 in dimensional regularization. In our calculations in dimension $d = 4-2\epsilon$, only three gamma matrix structures involving γ_5 need to be handled. And in order to get the UV finite terms at the NLO in α_s, it is sufficient to rewrite them as [14,15]

$$\begin{aligned} \gamma_\rho\gamma_\alpha\Gamma_\mu \otimes \gamma^\rho\gamma^\alpha\Gamma^\mu &= (16+4X_R\epsilon)\Gamma_\mu \otimes \Gamma^\mu, \\ \Gamma_\mu\gamma_\rho\gamma_\alpha \otimes \gamma^\alpha\gamma^\rho\Gamma^\mu &= (4+4Y_R\epsilon)\Gamma_\mu \otimes \Gamma^\mu, \\ \Gamma_\mu \otimes \gamma_\rho\gamma_\alpha\Gamma^\mu\gamma^\alpha\gamma^\rho &= (4+4Z_R\epsilon)\Gamma_\mu \otimes \Gamma^\mu, \end{aligned} \tag{13}$$

where Γ_μ represents the electroweak vertex $\gamma_\mu(1-\gamma_5)$, and the scheme dependence of γ_5 is fully reproduced by that of X_R, Y_R and Z_R. We use both the naive-dimensional-regularization (NDR) and the 't Hooft–Veltman (HV) scheme in our calculation, which corresponds to the parameters

$$\begin{aligned} &\text{NDR scheme:}\ X_R = -1, \qquad Y_R = Z_R = -2; \\ &\text{HV scheme:}\ X_R = -1, \qquad Y_R = Z_R = 0. \end{aligned} \tag{14}$$

Having subtracted the UV divergences, we turn to the treatment of the IR ones. There are three types of IR divergences in our calculations. They are the soft and collinear divergences, and also the Coulomb singularity in diagram (v_3) when the charm and anticharm quarks share the same momentum. The emergence of Coulomb singularity is a typical feature of the one-loop QCD corrections to $c\bar{c}$ vertex in a nonrelativistic configuration, which should be reproduced in the NRQCD calculations [11], and then

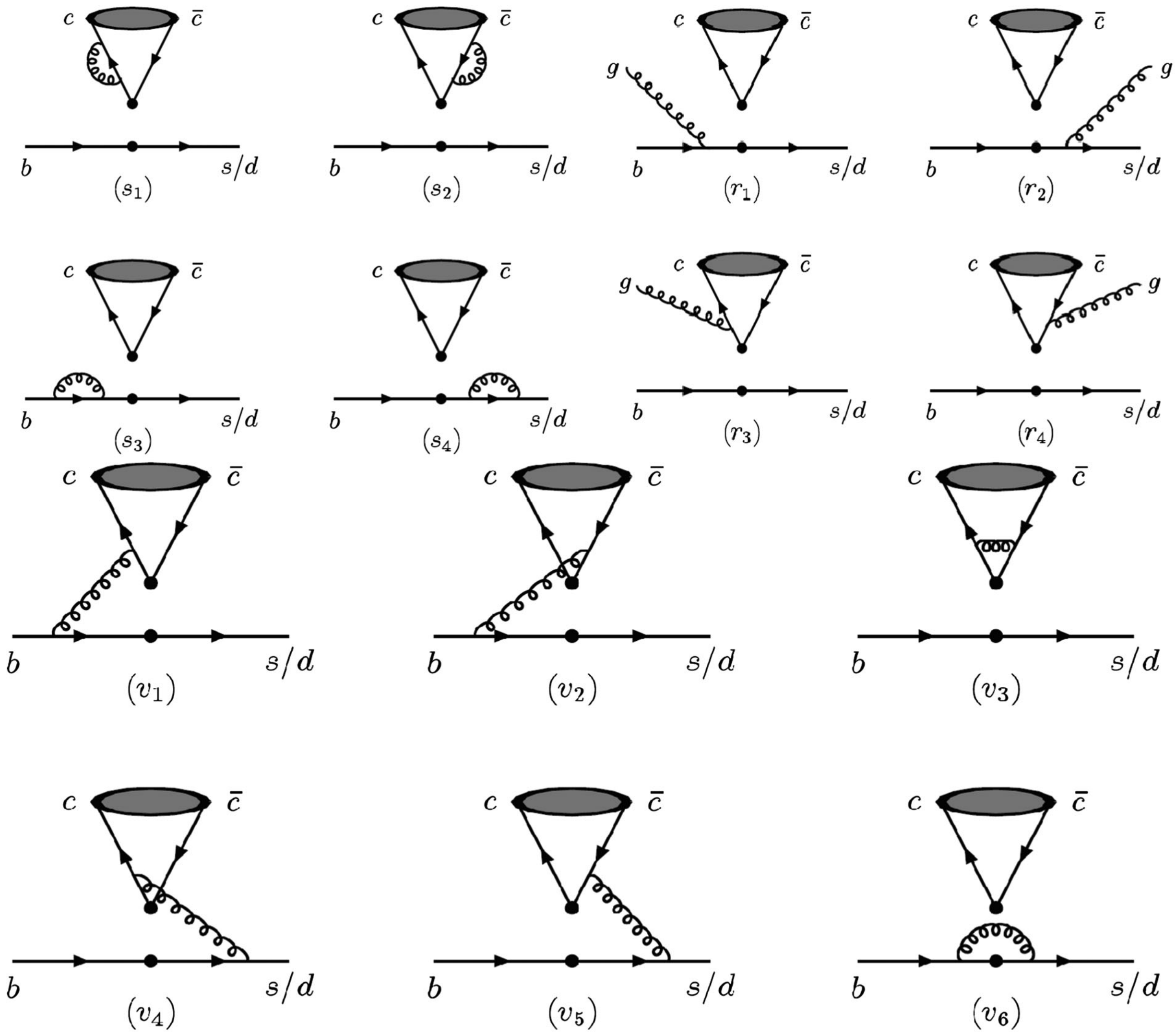

FIG. 1. Feynman diagrams of the NLO QCD corrections for the process $b \to H[c\bar{c}] + s/d$, where $(s_{1\text{–}4})$, $(v_{1\text{–}6})$ and $(r_{1\text{–}4})$ are the self-energy, vertex correction and real correction diagrams, respectively.

absorbed into the matrix element by redefinition of the operator in NRQCD (see Refs. [14] and [15] for more details).

The other IR divergences are all regularized by the artificial gluon mass λ. After summing up all the diagrams in Fig. 1, the soft divergences are not canceled completely, leaving those associated with the real correction diagrams (r_3) and (r_4) in Fig. 1 if the outgoing $c\bar{c}$ pair is in the ${}^3P_{J'}^{[8]}$,${}^3D_1^{[1]}$ and ${}^3D_2^{[1]}$ configurations. This fact is simply because the final state $c\bar{c}$ has been selected in a particular configuration, and then, is not inclusive enough to cancel the soft divergences. On the other hand, the uncanceled soft divergences are necessary for the NRQCD factorization [11], and they should be fully absorbed into the LDMEs by the renormalization of the operators in NRQCD.

To see the absorbtion of the extra soft divergences more explicitly, let us apply the NRQCD factorization formalism in (7) to the parton level decay process $b \to c\bar{c}[{}^3D_J^{[1]}]x$, and the partial decay width can be expressed as

$$\begin{aligned}\Gamma(b \to c\bar{c}[{}^3D_J^{[1]}]x) &= C({}^3S_1^{[1]})\langle\mathcal{O}_1({}^3S_1)\rangle + C({}^3S_1^{[8]})\langle\mathcal{O}_8({}^3S_1)\rangle \\ &\quad + \sum_{J'} C({}^3P_{J'}^{[8]})\langle\mathcal{O}_8({}^3P_{J'})\rangle + C({}^3D_J^{[1]})\langle\mathcal{O}_1({}^3D_J)\rangle.\end{aligned} \tag{15}$$

Here, the matrix elements should be understood as those for perturbative $c\bar{c}$ pairs in the corresponding nonrelativistic configurations, while the SDCs are just the same as those for ψ_J production since they are independent of the long-distance evolution of the $c\bar{c}$ pair into the physical state. Thus, the short-distance coefficient $C({}^3D_J^{[1]})$ in (15) can be obtained by matching the QCD partial decay width

$$\Gamma^{\rm QCD}(b\to c\bar{c}[^3D_J^{[1]}]x) = C^{\rm QCD}(^3D_J^{[1]})\langle\mathcal{O}_1(^3D_1)\rangle_{\rm Born} \tag{16}$$

onto the NRQCD one in (15). Here in (16), $\langle\mathcal{O}_1(^3D_J)\rangle_{\rm Born}$ denotes the tree level matrix element of perturbative $c\bar{c}[^3D_J^{[1]}]$, and $C^{\rm QCD}(^3D_J^{[1]})(J=1,2)$ have extra soft divergences proportional to $\ln(\lambda^2/m_b^2)$ after the UV and Coulomb subtractions, as have been mentioned above.

The operator $\mathcal{O}_8(^3P_{J'})$ can be mixed with $\mathcal{O}_1(^3D_J)$ at the NLO in α_s through the perturbative NRQCD diagrams shown in Fig. 2. Calculating these diagrams by using the Feynman rules in NRQCD [11], the mixing can be expressed as the relation between matrix elements:

$$\langle\mathcal{O}_8(^3P_{J'})\rangle^{(1)} = -\frac{\alpha_s}{4\pi}\left(\ln\frac{\lambda^2}{\mu_\Lambda^2}+\frac{1}{3}\right)\frac{16}{3}C_F \times\sum_J C_{J'J}\frac{\langle\mathcal{O}_1(^3D_J)\rangle^{(0)}}{2N_c m_c^2}, \tag{17}$$

where $C_F=4/3$, $N_C=3$ and $C_{J'J}$ are the generalized Clebsch-Gordan coefficients between $^3P_{J'}$ and ^3D_J, which had been calculated in Ref. [6] and are listed in Table I, the superscript (1)/(0) denotes a matrix element at one-loop/tree level, and μ_Λ is the NRQCD factorization scale introduced through the $\overline{\rm MS}$ subtraction of the UV divergences in the dimensional regularization. Moreover, the equality in (17) should be understood on the condition that the Coulomb singularities in the corrections of operator $\mathcal{O}_8(^3P_{J'})$ have been fully subtracted. Substituting the LO coefficients $C(^3P_{J'}^{[8]})$ obtained in the last section and the matrix elements in Eq. (17) into Eq. (15), one can get the same IR divergences as those in the QCD results in (16). This is a general feature of a low-energy effective theory such as NRQCD, which should fully reproduce the QCD results at the low-energy region. Therefore, the finite

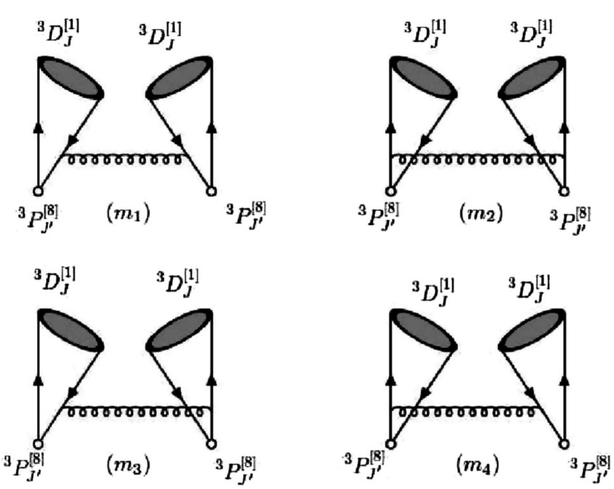

FIG. 2. The perturbative NRQCD diagrams of the mixing between the operator $\mathcal{O}_8(^3P_{J'})$ and $\mathcal{O}_1(^3D_J)$ at the NLO in α_s.

TABLE I. The Clebsch-Gordan coefficient between $^3P_{J'}$ and ^3D_J.

$C_{J'J}$	$^3P_0$	$^3P_1$	$^3P_2$
$^3D_1$	$\frac{5}{9}$	$\frac{5}{12}$	$\frac{1}{36}$
$^3D_2$	0	$\frac{3}{4}$	$\frac{1}{4}$
$^3D_3$	0	0	1

coefficient $C(^3D_J^{[1]})$ at the NLO in α_s can be obtained by matching (16) onto (15). The results are listed in Appendix B as coefficients g_{1-3} in the notation in (9). Similarly, the NLO coefficients $C(^3P_{J'}^{[8]})$ can be obtained with the help of the following matrix element relations in NRQCD:

$$\begin{aligned}\langle\mathcal{O}_1(^3S_1)\rangle^{(1)} &= -\frac{\alpha_s}{4\pi}\left(\ln\frac{\lambda^2}{\mu_\Lambda^2}+\frac{1}{3}\right)\frac{16}{3}\frac{\sum_{J'}\langle\mathcal{O}_8(^3P_{J'})\rangle^{(0)}}{m_c^2},\\ \langle\mathcal{O}_8(^3S_1)\rangle^{(1)} &= -\frac{\alpha_s}{4\pi}\left(\ln\frac{\lambda^2}{\mu_\Lambda^2}+\frac{1}{3}\right)\frac{16}{3}B_F\frac{\sum_{J'}\langle\mathcal{O}_8(^3P_{J'})\rangle^{(0)}}{m_c^2},\end{aligned} \tag{18}$$

where $B_F=5/12$. These coefficients and those for $n={}^3S_1^{[1]},{}^3S_1^{[8]}$, which had been calculated in Ref. [14], are also listed in Appendix B.

It needs to be emphasized that the coefficients for the $^3P_{J'}^{[8]}$, $^3D_1^{[1]}$ and $^3D_2^{[1]}$ configurations are μ_Λ dependent after matching, which will be canceled by the μ_Λ dependence of the LDMEs of $^3S_1^{[1]}$, $^3S_1^{[8]}$ and $^3P_{J'}^{[8]}$ order by order in α_s. Up to NLO in α_s, the μ_Λ evolution equations for these LDMEs can be derived from Eqs. (17) and (18), which are given by

$$\frac{d\langle\mathcal{O}_1(^3S_1)\rangle}{d\ln\mu_\Lambda} = \frac{\alpha_s}{4\pi}\frac{32}{3}\frac{\sum_{J'=0}^2\langle\mathcal{O}_8(^3P_{J'})\rangle}{m_c^2}, \tag{19a}$$

$$\frac{d\langle\mathcal{O}_8(^3S_1)\rangle}{d\ln\mu_\Lambda} = \frac{\alpha_s}{4\pi}\frac{32}{3}B_F\frac{\sum_{J'=0}^2\langle\mathcal{O}_8(^3P_{J'})\rangle}{m_c^2}, \tag{19b}$$

$$\frac{d\langle\mathcal{O}_8(^3P_{J'})\rangle}{d\ln\mu_\Lambda} = \frac{\alpha_s}{4\pi}\frac{32}{3}C_{J'J}C_F\frac{\langle\mathcal{O}_1(^3D_J)\rangle}{2N_c m_c^2}. \tag{19c}$$

B. Estimation of LDMEs

The color-singlet LDMEs for $^3D_J^{[1]}$ can be related to the second derivative of the radial wave function at the origin

$$\begin{aligned}\langle\mathcal{O}_1^{\psi_J}(^3D_J)\rangle &= (2J+1)\langle 1^3D_J|\mathcal{O}_1(^3D_J)|1^3D_J\rangle\\ &= (2J+1)(2N_c)\frac{15|R''_{1D}(0)|^2}{8\pi},\end{aligned} \tag{20}$$

where $|R''_{1D}(0)|^2$ can be estimated by the potential models. The matrix element $\langle\mathcal{O}_1^{\psi_{J'}}(^3D_J)\rangle = 0$ for $J'\neq J$ at the LO in v^2. As for other LDMEs, there is little information from experiments and model calculations. In Ref. [12], the LDMEs were estimated by the naive velocity scaling rules (VSRs)

$$\langle \mathcal{O}_8^{\psi_1}(^3S_1)\rangle \approx \frac{\langle \mathcal{O}_8^{\psi_1}(^3P_1)\rangle}{m_c^2} \approx \frac{\langle \mathcal{O}_1^{\psi_1}(^3D_1)\rangle}{m_c^4}, \tag{21}$$

and the spin symmetry relations

$$\langle \mathcal{O}_8^{\psi_J}(^3S_1)\rangle = \frac{2J+1}{3}\langle \mathcal{O}_8^{\psi_1}(^3S_1)\rangle, \tag{22a}$$

$$\langle \mathcal{O}_8^{\psi_J}(^3P_1)\rangle = \frac{2J+1}{3}\langle \mathcal{O}_8^{\psi_1}(^3P_1)\rangle. \tag{22b}$$

Similar relations are also used to estimate the LDMEs in Ref. [13]. However, these relations tend to overestimate the LDMEs and even provide the wrong pattern sometimes for a reason which will be explained below.

Dynamically, the relations in (21) and (22) come from the power counting for the soft gluon interactions in NRQCD [11], which cause the mixing between operators indicated by the evolution equations in (19). The color factor $1/(2N_c) = 1/6$ in (19c) tends to suppress the CO matrix element $\langle \mathcal{O}_8^{\psi_1}(^3P_1)\rangle$ relative to that in the naive relation in (21). A similar suppression relative to the naive VSRs for the CO matrix element was also found in J/ψ and η_c production at hadron colliders, where the suppression factor of the CO matrix element to the CS one is about $1/100$ [17] while in the naive VSRs it would be of order $v^4 \sim 1/15$. Moreover, the nonuniversal coefficient $C_{J'J}$ in (19c) will violate the naive spin symmetry relation in (22b). For example, $\langle \mathcal{O}_8^{\psi_3}(^3P_1)\rangle = 0$ at leading order in v^2 since $C_{13} = 0$ for the single gluon transition in NRQCD.

On the other hand, the LDMEs can be roughly estimated by solving the evolution equations in (19) in the leading logarithm approximation. That is, for the evolution of the LDMEs from the scale $\mu_{\Lambda_0} \sim m_c v$ to the factorization scale $\mu_\Lambda \sim m_c \gg \mu_{\Lambda_0}$, one can neglect the initial values at μ_{Λ_0}, and the solutions of the equations in (19) will be given by

$$\langle \mathcal{O}_1(^3S_1)\rangle(\mu_\Lambda) = \frac{1}{2N_c}\frac{3C_F}{2}\left(\frac{8}{3\beta_0}\ln\frac{\alpha_s(\mu_{\Lambda_0})}{\alpha_s(\mu_\Lambda)}\right)^2 \frac{\langle \mathcal{O}_1(^3D_1)\rangle}{m_c^4}, \tag{23a}$$

$$\langle \mathcal{O}_8(^3S_1)\rangle(\mu_\Lambda) = \frac{1}{2N_c}\frac{3C_F B_F}{2}\left(\frac{8}{3\beta_0}\ln\frac{\alpha_s(\mu_{\Lambda_0})}{\alpha_s(\mu_\Lambda)}\right)^2 \frac{\langle \mathcal{O}_1(^3D_1)\rangle}{m_c^4}, \tag{23b}$$

$$\langle \mathcal{O}_8(^3P_{J'})\rangle(\mu_\Lambda) = \frac{1}{2N_c}C_F C_{J'J}\left(\frac{8}{3\beta_0}\ln\frac{\alpha_s(\mu_{\Lambda_0})}{\alpha_s(\mu_\Lambda)}\right) \frac{\langle \mathcal{O}_1(^3D_J)\rangle}{m_c^2}, \tag{23c}$$

where $\beta_0 = \frac{11C_A}{6} - \frac{N_f}{3}$, $C_A = 3$ and $N_f = 3$. This method was first proposed by the authors of Ref. [18] to reduce the freedom of the CO matrix elements in Υ annihilation decay and recently developed in D-wave cases [6,15,19]. The evolution method has been numerically checked in h_c light hadronic decay by comparing its result with that obtained by extraction from experimental data, and they were found to be consistent within about 30% error [20]. Here, we will use the results in (23) to estimate the relevant LDMEs by treating the CS ones $\langle \mathcal{O}_1(^3D_J)\rangle$ in (20) as input. The uncertainties from neglecting the initial values for these LDMEs can be partly estimated by varying the value of the starting scale μ_{Λ_0}.

IV. RESULTS AND DISCUSSIONS

We choose $|R''_{1D}(0)|^2 = 0.015\ \mathrm{GeV}^7$ according to the Buchmuller-Tye potential model model [21] and $m_c = 1.5$ GeV to estimate the CS LDMEs $\langle \mathcal{O}_1(^3D_J)\rangle$ in (20), and the results are listed in Table II. As for other LDMEs, we evaluate them at NRQCD factorization scale $\mu_\Lambda = 2m_c$ by using the solutions in (23) with the starting scale $\mu_{\Lambda_0} = m_c v = 750$ MeV for $v^2 = 0.25$. The results are also listed in Table II.

The numerical results of the LO and the NLO SDCs are shown in Table III with three different choices of the renormalization scale $\mu = m_b/2, m_b, 2m_b$, where $m_b = 4.8$ GeV. The LO and NLO Wilson coefficients in the weak effective Hamiltonian in (5) are evaluated by the formulas shown in Ref. [22]. From Table III, one can see that the coefficients for $^3P_1^{[8]}$ and $^3S_1^{[8]}$ are evidently larger than the others. This is simply because they receive large contributions from tree level diagrams, which are proportional to $C_{[8]}^2$.

Using the NLO SDCs at $\mu = m_b$ in Table III and the LDMEs in Table II, one can evaluate the branching ratios

TABLE II. The relevant LDMEs (in units of GeV^3) at NRQCD factorization scale $\mu_\Lambda = 2m_c$, where $m_c = 1.5$ GeV.

States	$\frac{\langle \mathcal{O}(^3D_1^{[1]})\rangle}{m_c^4}$	$\frac{\langle \mathcal{O}(^3D_2^{[1]})\rangle}{m_c^4}$	$\frac{\langle \mathcal{O}(^3D_3^{[1]})\rangle}{m_c^4}$	$\frac{\langle \mathcal{O}(^3P_0^{[8]})\rangle}{m_c^2}$	$\frac{\langle \mathcal{O}(^3P_1^{[8]})\rangle}{m_c^2}$	$\frac{\langle \mathcal{O}(^3P_2^{[8]})\rangle}{m_c^2}$	$\langle \mathcal{O}(^3S_1^{[1]})\rangle$	$\langle \mathcal{O}(^3S_1^{[8]})\rangle$
ψ_1	0.032	0	0	0.0029	0.0022	0.0001	0.0019	0.0008
ψ_2	0	0.053	0	0	0.0065	0.0022	0.0031	0.0013
ψ_3	0	0	0.074	0	0	0.012	0.0044	0.0018

TABLE III. The LO and NLO SDCs in the NDR and HV schemes. The QCD renormalization scale μ is taken to be $m_b/2, m_b, 2m_b$, and $m_b = 4.8$ GeV, $m_c = 1.5$ GeV.

Fock state	LO			NLO NDR scheme			NLO HV scheme		
μ	$m_b/2$	m_b	$2m_b$	$m_b/2$	m_b	$2m_b$	$m_b/2$	m_b	$2m_b$
${}^3D_1^{[1]}$	0.0014	0.0335	0.0863	−0.5197	−0.4148	−0.3580	−0.4567	−0.3456	−0.2865
${}^3D_2^{[1]}$	0	0	0	−0.8590	−0.6023	−0.4631	−0.7994	−0.5585	−0.4275
${}^3D_3^{[1]}$	0	0	0	0.0025	0.0017	0.0013	0.0023	0.0016	0.0012
${}^3P_0^{[8]}$	0	0	0	−1.309	−0.988	−0.827	−1.196	−0.8888	−0.7375
${}^3P_1^{[8]}$	10.918	9.780	9.060	15.11	13.21	11.97	15.86	13.59	12.13
${}^3P_2^{[8]}$	0	0	0	−1.056	−0.7978	−0.6677	−0.9651	−0.7175	−0.5954
${}^3S_1^{[1]}$	0.0034	0.0805	0.2072	−0.1168	−0.2425	−0.3138	−0.0288	−0.1167	−0.1715
${}^3S_1^{[8]}$	5.459	4.890	4.530	7.340	6.346	5.711	7.708	6.531	5.787

for the semi-inclusive B decays into ψ_J. To estimate the uncertainties from the factorization scale $\mu_\Lambda = 2m_c$ and the LDMEs, we vary m_c and μ_{Λ_0}, respectively, in the ranges (1.4, 1.6) GeV and (700, 800) MeV, which will be shown as errors in the following results.

Let us first consider the production rate of ψ_1, which is believed to be the dominant component of $\psi(3770)$. The branching ratios in the NDR and HV schemes are

$$\begin{aligned} \mathrm{Br}(B\to\psi_1X)_{\mathrm{NDR}} &= (5.09^{+2.51}_{-1.87})\times10^{-4}, \\ \mathrm{Br}(B\to\psi_1X)_{\mathrm{HV}} &= (6.21^{+2.96}_{-2.19})\times10^{-4}, \end{aligned} \tag{24}$$

respectively, where the dominant contributions come from the CO channel ${}^3P_1^{[8]}$. The results in (24) are only slightly larger than the branching ratio of the exclusive decay $B\to\psi(3770)K$ in (3), and could be too small to account for the ratio $R_2(\psi(3770))$ defined in (4), which is expected to be no more than 1/10. One might think that the $\psi(3770)$ could produce in B decays predominantly through its $\psi(2S)$ component. However, the 2S-1D mixing angle θ is only about -12° in the notation [23–25]

$$\begin{aligned} \psi(3686) &= \cos\theta\psi(2S) + \sin\theta\psi_1, \\ \psi(3770) &= \cos\theta\psi_1 - \sin\theta\psi(2S). \end{aligned} \tag{25}$$

Thus, by using the PDG data $\mathrm{Br}(B\to\psi(3686)X) = (3.07\pm0.21)\times10^{-3}$ [8], the inclusive branching ratio of B decay into $\psi(3770)$ through the $\psi(2S)$ component would be

$$\begin{aligned} \sin^2\theta\mathrm{Br}(B\to\psi(2S)X) &\approx \sin^2\theta\mathrm{Br}(B\to\psi(3686)X) \\ &= (1.33\pm0.09)\times10^{-4}, \end{aligned} \tag{26}$$

which is even smaller than those in (24). In total, the predicted ratio $R_2(\psi(3770)) = (0.5–1)$ is substantially larger than one expects, especially when the production rates in (24) mainly come from the CO channel ${}^3P_1^{[8]}$.

The inclusive production rate of ψ_2 in B decay is predicted to be

$$\begin{aligned} \mathrm{Br}(B\to\psi_2X)_{\mathrm{NDR}} &= (1.79^{+0.81}_{-0.62})\times10^{-3}, \\ \mathrm{Br}(B\to\psi_2X)_{\mathrm{HV}} &= (1.96^{+0.92}_{-0.68})\times10^{-3}, \end{aligned} \tag{27}$$

where the dominant contributions come also from the CO channel ${}^3P_1^{[8]}$. The results in (27) are about 2 orders of magnitude larger than the exclusive one in (2). In other words, the ratio $R_2(\psi_2)\sim0.01$, which is consistent with the one for another tensor meson χ_{c2}, of which $R_2(\chi_{c2}) = (0.7\pm0.3)\times10^{-2}$ [8]. The inclusive decay $B\to\psi_2X$ may be measured directly by the LHCb or Belle II collaborations in the future, since the predicted branching ratios in (27) are large, and the decay mode $\chi_{c1}\gamma$ for ψ_2 is expected to be dominant.

As for the production of ψ_3, the rates are predicted to be

$$\begin{aligned} \mathrm{Br}(B\to\psi_3X)_{\mathrm{NDR}} &= (0.33^{+0.60}_{-0.38})\times10^{-4}, \\ \mathrm{Br}(B\to\psi_3X)_{\mathrm{HV}} &= (0.89^{+0.80}_{-0.53})\times10^{-4}, \end{aligned} \tag{28}$$

which are much smaller than those for ψ_1 and ψ_2. This smallness occurs for the following reasons. First, for the ${}^3P_1^{[8]}$ channel the short-distance coefficient is the largest but the corresponding matrix element $\langle\mathcal{O}_8^{\psi_3}({}^3P_1)\rangle = 0$ at leading order in v^2. Furthermore, the extreme smallness of the central values in (28) is the consequence of the cancellation between contributions of the ${}^3S_1^{[8]}$ and ${}^3P_2^{[8]}$ channels. Considering the large uncertainties in the estimation of the LDMEs, the cancellation may be somewhat accidental, and we will use a single channel, say, ${}^3S_1^{[8]}$ alone to estimate the upper limit of the production rate of ψ_3. The results read

$$\mathrm{Br}(B \to \psi_3 X)^{{}^3S_1^{[8]}}_{\mathrm{NDR}} = 3.53 \times 10^{-4},$$
$$\mathrm{Br}(B \to \psi_3 X)^{{}^3S_1^{[8]}}_{\mathrm{HV}} = 3.63 \times 10^{-4}, \tag{29}$$

which can also be treated as a rough estimation for the order of magnitude of the branching ratio. Phenomenologically, the phase space allowed in open-charmed decay $\psi_3 \to D\bar{D}$ is a D-wave process, the partial decay width $\Gamma(\psi_3 \to D\bar{D}) \sim 0.5$ MeV for $m(\psi_3) = 3806$ MeV [26], and would be no more than 1 MeV for $m(\psi_3) < 3830$ MeV, which is estimated by simply changing the phase space factor. Thus, the missing state ψ_3 is expected to be narrow. On the other hand, the partial decay width $\Gamma(\psi_3 \to \text{light hadrons}) \sim 0.2\,\text{MeV}$ [6], which is compared with that of $\Gamma(\psi_3 \to \gamma\chi_{c2}) \sim 0.3$ MeV [7,26]. Therefore, one can expect that the missing state ψ_3 can be searched for in B decays through the cascade decay $\psi_3 \to \gamma\chi_{c2} \to \gamma\gamma J/\psi$ by the LHCb or Belle II collaborations in the future. On the other hand, comparing the measurement with our prediction is important for both testing the NRQCD factorization approach and determining the LDMEs.

The above results are only evaluated at the fixed renormalization scale $\mu = m_b$. The scale dependence of the branching ratios $\mathrm{Br}(B \to \psi_J X)$ for $J = 1$, 2 and 3 are shown in Figs. 3, 4 and 5, respectively.

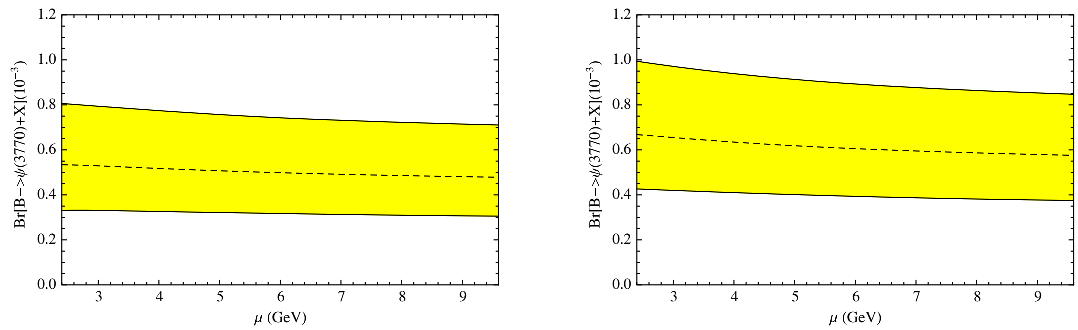

FIG. 3 (color online). QCD renormalization scale μ dependence of $\mathrm{Br}[B \to \psi(3770)X]$ in the NDR scheme (left panel) and in the HV scheme (right panel). μ ranges from $\frac{m_b}{2}$ to $2m_b$.

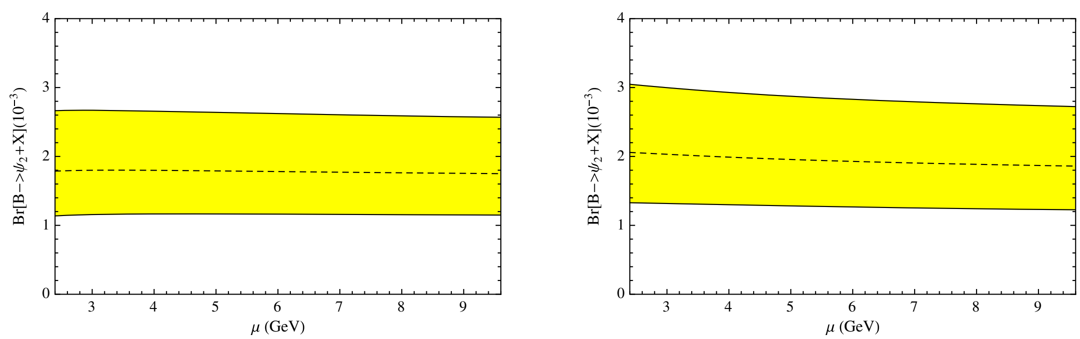

FIG. 4 (color online). QCD renormalization scale μ dependence of $\mathrm{Br}[B \to \psi_2 X]$ in the NDR scheme (left panel) and in the HV scheme (right panel). μ ranges from $\frac{m_b}{2}$ to $2m_b$.

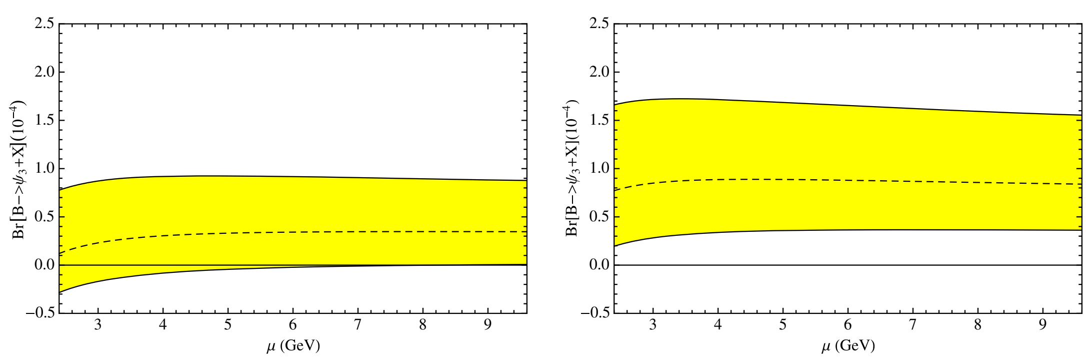

FIG. 5 (color online). QCD renormalization scale μ dependence of $\mathrm{Br}[B \to \psi_3 X]$ in the NDR scheme (left panel) and in the HV scheme (right panel). μ ranges from $\frac{m_b}{2}$ to $2m_b$.

V. SUMMARY

In summary, we study the semi-inclusive decays of the B meson into spin-triplet D-wave chamonium states $\psi_J(J=1,2,3)$ within the framework of NRQCD factorization [11] at NLO in α_s and LO in v^2. The finite short-distance coefficients for ${}^3D_J^{[1]}$ channels are obtained for he first time, and the IR divergences in the QCD calculations for these channels are absorbed into the redefinitions of the NRQCD LDMEs for the ${}^3P_{J'}^{[8]}(J'=0,1,2)$ channels. The LDMEs for the ${}^3D_J^{[1]}$ channels are estimated with the help of a potential model, and other LDMEs are obtained by solving the evolution equations in the leading logarithm approximation, which tend to count correctly for the spin-coupling factors $C_{J'J}$ between the ${}^3P_{J'}^{[8]}$ and ${}^3D_J^{[1]}$ states.

The branching ratios $\mathrm{Br}(B\to\psi_{1,2}X)$ are predicted to be about 6×10^{-4} and 2×10^{-3}, respectively. The relative errors for the above predictions are both about 50%, which mainly come from the uncertainties of the LDMEs. The branching ratio $\mathrm{Br}(B\to\psi_3X)$ can be very small due to the cancellation between the ${}^3S_1^{[8]}$ and ${}^3P_2^{[8]}$ channels. Thus, we use the single channel ${}^3S_1^{[8]}$ alone to set up the upper limit for $\mathrm{Br}(B\to\psi_3X)$, which is about 4×10^{-4}. The above predictions may deserve to be compared with the future measurements to test the NRQCD factorization formula and to determine the LDMEs further. In particular, the decay $B\to\psi_3X$ may be used to search for the missing state ψ_3 through the cascade decay $\psi_3\to\gamma\chi_{c2}\to\gamma\gamma J/\psi$, and the measurement on $\mathrm{Br}(B\to\psi(3770)X)$ will provide new information for understanding the large production rate of $\psi(3770)$ in exclusive B decays if it is dominated by the ψ_1 component.

ACKNOWLEDGMENTS

We would like to thank Yan-Qing Ma for the many helpful discussions. This work was supported in part by the National Natural Science Foundation of China (Grants No. 11075002, No. 11021092, No. 11475005) and the National Key Basic Research Program of China (Grant No. 2015CB856700).

APPENDIX A: THE DEFINITIONS OF RELEVANT OPERATORS

The relevant operators for inclusive production of charmonium state H are defined as

$$\mathcal{O}^H({}^3S_1^{[1]})=\chi^\dagger\sigma^i\psi(a_H^\dagger a_H)\psi^\dagger\sigma^i\chi, \tag{A1}$$

$$\mathcal{O}^H({}^3S_1^{[8]})=\chi^\dagger T^a\sigma^i\psi(a_H^\dagger a_H)\psi^\dagger T^a\sigma^i\chi, \tag{A2}$$

$$\mathcal{O}^H({}^3P_0^{[8]})=\chi^\dagger\left(-\frac{i}{2}\overleftrightarrow{D}\cdot\vec{\sigma}\right)T^a\psi(a_H^\dagger a_H)\psi^\dagger\left(-\frac{i}{2}\overleftrightarrow{D}\cdot\vec{\sigma}\right)T^a\chi, \tag{A3}$$

$$\begin{aligned}\mathcal{O}^H({}^3P_1^{[8]})=\chi^\dagger\left(-\frac{i}{2}\overleftrightarrow{D}\times\vec{\sigma}\right)T^a\psi(a_H^\dagger a_H)\\ \cdot\psi^\dagger\left(-\frac{i}{2}\overleftrightarrow{D}\times\vec{\sigma}\right)T^a\chi,\end{aligned} \tag{A4}$$

$$\begin{aligned}\mathcal{O}^H({}^3P_2^{[8]})=\chi^\dagger\left(-\frac{i}{2}\overleftrightarrow{D}^{(i}\vec{\sigma}^{j)}\right)T^a\psi(a_H^\dagger a_H)\\ \cdot\psi^\dagger\left(-\frac{i}{2}\overleftrightarrow{D}^{(i}\vec{\sigma}^{j)}\right)T^a\chi,\end{aligned} \tag{A5}$$

$$\mathcal{O}^H({}^3D_1^{[1]})=\frac{3}{5}\chi^\dagger K^i\psi(a_H^\dagger a_H)\psi^\dagger K^i\chi, \tag{A6}$$

$$\mathcal{O}^H({}^3D_2^{[1]})=\frac{1}{6}\chi^\dagger K^{ij}\psi(a_H^\dagger a_H)\psi^\dagger K^{ij}\chi, \tag{A7}$$

$$\mathcal{O}^H({}^3D_3^{[1]})=\frac{1}{3}\chi^\dagger K^{ijk}\psi(a_H^\dagger a_H)\psi^\dagger K^{ijk}\chi, \tag{A8}$$

where the spin tensor operator K's are given by

$$K^i=\sigma^jS^{ij}, \tag{A9}$$

$$K^{ij}=\epsilon^{ikl}\sigma^lS^{jk}+\epsilon^{jkl}\sigma^lS^{ik}, \tag{A10}$$

$$\begin{aligned}K^{ijk}=\sigma^iS^{jk}+\sigma^jS^{ki}+\sigma^kS^{ij}\\ -\frac{2}{5}\sigma^l(\delta^{jk}S^{il}+\delta^{ki}S^{jl}+\delta^{ij}S^{kl}),\end{aligned} \tag{A11}$$

$$S^{ij}=\left(\frac{-i}{2}\right)^2\left(\overleftrightarrow{D}^i\overleftrightarrow{D}^j-\frac{1}{3}\overleftrightarrow{D}^2\delta^{ij}\right). \tag{A12}$$

APPENDIX B: THE RELEVANT NLO SDCs

For ${}^3S_1^{[1]}$,

$$\begin{aligned}g_1[{}^3S_1^{[1]}]=&\frac{4}{9}(1-\eta)(3(10\eta^2+\eta-3)+4\pi^2(2\eta^2-\eta-1))-\frac{8}{3}(4\eta+5)(1-\eta)^2\ln(1-\eta)\\&-\frac{16}{3}(2\eta+1)(1-\eta)^2\ln\eta\ln(1-\eta)+\frac{16}{3}\eta(1+\eta)(2\eta-1)\ln\eta\\&-\frac{32}{3}(2\eta+1)(1-\eta)^2\mathrm{Li}_2(\eta)+\frac{16}{3}(2\eta+1)(1-\eta)^2Z_R,\end{aligned} \tag{B1}$$

$$g_2[{}^3S_1^{[1]}] = \frac{8(\eta-1)^3(\eta^2-3)}{3(\eta-2)^2}\ln(1-\eta) + \frac{4\eta^2(4\eta^2-19\eta+26)}{3(\eta-2)}\ln\eta - \frac{2(16\eta^4-67\eta^3+74\eta^2+11\eta-34)}{3(\eta-2)} - \frac{32\eta(\eta-1)^3}{3(\eta-2)}\ln 2$$
$$+ 4(2\eta+1)(1-\eta)^2\ln\left(\frac{m_b^2}{\mu^2}\right) - \frac{4}{3}(2\eta+1)(1-\eta)^2X_R + \frac{4}{3}(2\eta+1)(1-\eta^2)Y_R, \tag{B2}$$

$$g_3[{}^3S_1^{[1]}] = \frac{4}{27}(8\eta^3-45\eta^2+36\eta+1) + \frac{8}{9}(6\eta-1)\ln\eta. \tag{B3}$$

For ${}^3S_1^{[8]}$,

$$g_1[{}^3S_1^{[8]}] = \frac{4}{9}(8\eta^3-45\eta^2+36\eta+1) + \frac{8}{3}(6\eta-1)\ln\eta, \tag{B4}$$

$$g_2[{}^3S_1^{[8]}] = \frac{2(\eta^2-3)(\eta-1)^3\ln(1-\eta)}{(\eta-2)^2} + \frac{\eta^2(4\eta^2-19\eta+26)\ln(\eta)}{\eta-2} + \frac{-16\eta^4+67\eta^3-74\eta^2-11\eta+34}{2(\eta-2)} - \frac{8\eta(\eta-1)^3\ln(2)}{\eta-2}$$
$$+ 3(2\eta+1)(\eta-1)^2\ln\left(\frac{m_b^2}{\mu^2}\right) - (2\eta+1)(\eta-1)^2X_R + (2\eta+1)(\eta-1)^2Y_R, \tag{B5}$$

$$\begin{aligned} g_3[{}^3S_1^{[8]}] = &-\frac{(74\eta^2-83\eta-18)(\eta-1)^2\ln(2)}{\eta-2} \\ &+ \frac{(5228\eta^3-14795\eta^2+6\pi^2(58\eta^3-73\eta^2-79\eta-14)+5779\eta+5294)(\eta-1)}{36(\eta-2)} \\ &- \frac{(83\eta^3-291\eta^2+188\eta+110)(\eta-1)^2\ln(1-\eta)}{(\eta-2)^2} \\ &+ \frac{1}{6(\eta-2)}((426\eta^4-1158\eta^3+216\eta^3\ln(2)+1062\eta^2-540\eta^2\ln(2)-547\eta \\ &+ 108\eta\ln(2)-34+216\ln(2))\ln(\eta)) - \frac{9}{2}(2\eta+1)(\eta-1)^2\ln^2(2-\eta) \\ &+ 9(2\eta+1)(\eta-1)^2\ln(1-\eta)\ln(2-\eta) - 18(2\eta+1)(\eta-1)\ln(2)\ln(2-\eta) \\ &- 2(2\eta+1)(4\eta+5)(\eta-1)\ln(1-\eta)\ln(\eta) - 6(2\eta+1)(\eta-1)^2\ln\left(\frac{m_b^2}{\mu^2}\right) \\ &- 9(\eta+1)(2\eta+1)(\eta-1)\mathrm{Li}_2\left(\frac{\eta-1}{\eta-2}\right) + 18(2\eta+1)(\eta-1)\mathrm{Li}_2\left(\frac{2(\eta-1)}{\eta-2}\right) \\ &- (2\eta+1)(7\eta+29)(\eta-1)\mathrm{Li}_2(\eta) + 2(2\eta+1)(\eta-1)^2X_R \\ &+ 7(2\eta+1)(\eta-1)^2Y_R - (2\eta+1)(\eta-1)^2Z_R. \end{aligned} \tag{B6}$$

For ${}^3P_0^{[8]}$,

$$g_1[{}^3P_0^{[8]}] = -\frac{4}{3}(18\eta^3-5\eta^2-38\eta+25) - \frac{16}{3}(2\eta+1)(\eta-1)^2\ln\left(\frac{\mu_\Lambda^2}{4m_c^2}\right)$$
$$+ \frac{32}{3}(2\eta+1)\left(\eta-1)^2\ln(1-\eta) - \frac{8}{3}(8\eta^3-12\eta^2+1)\ln(\eta)\right), \tag{B7}$$

$$g_2[{}^3P_0^{[8]}] = 0, \tag{B8}$$

$$g_3[{}^3P_0^{[8]}] = \frac{1}{3}(-42\eta^3 - \eta^2 + 122\eta - 79) - \frac{10}{3}(2\eta+1)(\eta-1)^2 \ln\left(\frac{\mu_\Lambda^2}{4m_c^2}\right) + \frac{20}{3}(2\eta+1)(\eta-1)^2\ln(1-\eta) - \frac{2}{3}(20\eta^3 - 30\eta^2 + 7)\ln(\eta). \tag{B9}$$

For ${}^3P_1^{[8]}$,

$$g_1[{}^3P_1^{[8]}] = -\frac{16}{3}(2\eta-1)(2\eta^2-2\eta-1)\ln(\eta) - \frac{8}{9}(56\eta^3 - 93\eta^2 + 24\eta + 13) + \frac{32}{3}(2\eta+1)(\eta-1)^2\ln(1-\eta) - \frac{16}{3}(2\eta+1)(\eta-1)^2\ln\left(\frac{\mu_\Lambda^2}{4m_c^2}\right), \tag{B10}$$

$$\begin{aligned} g_2[{}^3P_1^{[8]}] = &-16\eta^2\ln(2)\ln(2-\eta) - 16\eta^2\ln(1-\eta)\ln(\eta) \\ &+ \frac{2\eta^2(12\eta^3 - 59\eta^2 + 8\eta^2\ln(2) + 96\eta - 32\eta\ln(2) - 48 + 32\ln(2))\ln(\eta)}{(\eta-2)^2} \\ &- \frac{8\eta^2(4\eta^3 - 21\eta^2 + 38\eta - 25)\ln(2)}{(\eta-2)^2} - \frac{4(3\eta^4 - 10\eta^3 + 8\eta^2 + 3)(\eta-1)\ln(1-\eta)}{(\eta-2)^2} \\ &+ \frac{24\eta^5 + (16\pi^2 - 63)\eta^4 - 16(3+4\pi^2)\eta^3 + (123 + 64\pi^2)\eta^2 - 24\eta(\ln(16) - 7) - 204}{3(\eta-2)^2} + 6(2\eta+1)(\eta-1)^2\ln\left(\frac{m_b^2}{\mu^2}\right) \\ &- 16\eta^2\mathrm{Li}_2\left(\frac{\eta-1}{\eta-2}\right) + 16\eta^2\mathrm{Li}_2\left(\frac{2(\eta-1)}{\eta-2}\right) \\ &- 32\eta^2\mathrm{Li}_2(\eta) - 2(2\eta+1)(\eta-1)^2X_R + 2(2\eta+1)(\eta-1)^2Y_R, \end{aligned} \tag{B11}$$

$$\begin{aligned} g_3[{}^3P_1^{[8]}] = &-4(8\eta^3 + 16\eta^2 - 9\eta - 5)\ln(1-\eta)\ln(\eta) \\ &+ \frac{1}{18(\eta-2)}(5011\eta^4 - 17939\eta^3 + 15135\eta^2 + 6\pi^2(58\eta^4 - 91\eta^3 - 86\eta^2 + 65\eta + 14) \\ &+ 1907\eta - 4114) - \frac{10(47\eta^4 - 210\eta^3 + 251\eta^2 - 18\eta - 58)(\eta-1)\ln(1-\eta)}{3(\eta-2)^2} \\ &- \frac{2(58\eta^4 - 269\eta^3 + 399\eta^2 - 112\eta - 36)(\eta-1)\ln(2)}{(\eta-2)^2} + \frac{1}{3(\eta-2)^2}(398\eta^5 - 1838\eta^4 + 336\eta^4\ln(2) + 2669\eta^3 \\ &- 1452\eta^3\ln(2) - 835\eta^2 + 1668\eta^2\ln(2) - 368\eta + 68 - 432\ln(2))\ln(\eta) \\ &- 9(2\eta+1)(\eta-1)^2\ln^2(2-\eta) + 18(2\eta+1)(\eta-1)^2\ln(1-\eta)\ln(2-\eta) \\ &- 4(4\eta-3)(7\eta+3)\ln(2)\ln(2-\eta) - 12(2\eta+1)(\eta-1)^2\ln\left(\frac{m_b^2}{\mu^2}\right) - \frac{10}{3}(2\eta+1)(\eta-1)^2\ln\left(\frac{\mu_\Lambda^2}{4m_c^2}\right) \\ &- 2(18\eta^3 + 29\eta^2 - 18\eta - 9)\mathrm{Li}_2\left(\frac{\eta-1}{\eta-2}\right) \\ &- 2(14\eta^3 + 91\eta^2 - 36\eta - 29)\mathrm{Li}_2(\eta) + 4(4\eta-3)(7\eta+3)\mathrm{Li}_2\left(\frac{2(\eta-1)}{\eta-2}\right) \\ &+ 4(2\eta+1)(\eta-1)^2X_R + 14(2\eta+1)(\eta-1)^2Y_R - 2(2\eta+1)(\eta-1)^2Z_R. \end{aligned} \tag{B12}$$

For ${}^3P_2^{[8]}$,

$$g_1[{}^3P_2^{[8]}] = -\frac{8}{15}(76\eta^3 - 107\eta^2 + 4\eta + 27) - \frac{16}{15}(20\eta^3 - 30\eta^2 + 1)\ln(\eta) + \frac{32}{3}(2\eta+1)(\eta-1)^2\ln(1-\eta) - \frac{16}{3}(2\eta+1)(\eta-1)^2\ln\left(\frac{\mu_\Lambda^2}{4m_c^2}\right), \tag{B13}$$

$$g_2[{}^3P_2^{[8]}] = 0, \tag{B14}$$

$$g_3[{}^3P_2^{[8]}] = \frac{1}{30}(-721\eta^3 + 854\eta^2 + 149\eta - 282) + \frac{1}{15}(-200\eta^3 + 300\eta^2 + 81\eta - 28)\ln(\eta) + \frac{20}{3}(2\eta+1)(\eta-1)^2\ln(1-\eta) - \frac{10}{3}(2\eta+1)(\eta-1)^2\ln\left(\frac{\mu_\Lambda^2}{4m_c^2}\right). \tag{B15}$$

For ${}^3D_1^{[1]}$,

$$g_1[{}^3D_1^{[1]}] = -\frac{5}{27}(3(-6\eta^2+9\eta+5) + \pi^2(8\eta^2-4\eta-4))(\eta-1) - \frac{10}{9}(4\eta+5)(\eta-1)^2\ln(1-\eta) - \frac{20}{9}(2\eta+1)(\eta-1)^2\ln(1-\eta)\ln(\eta) + \frac{20}{9}\eta(\eta+1)(2\eta-1)\ln(\eta) - \frac{40}{9}(2\eta+1)(\eta-1)^2\mathrm{Li}_2(\eta) + \frac{20}{9}(2\eta+1)(\eta-1)^2 Z_R, \tag{B16}$$

$$\begin{aligned} g_2[{}^3D_1^{[1]}] = &-\frac{80}{9}\eta^2\ln(2)\ln(2-\eta) - \frac{80}{9}\eta^2\ln(1-\eta)\ln(\eta) \\ &+ \frac{1}{9(\eta-2)^3}(\eta^2(84\eta^4 - 567\eta^3 + 80\eta^3\ln(2) + 1350\eta^2 - 480\eta^2\ln(2) \\ &- 1200\eta + 960\eta\ln(2) + 240 - 640\ln(2))\ln(\eta)) + \frac{8\eta(83\eta^4 - 225\eta^3 + 235\eta^2 - 40\eta - 54)\ln(2)}{9(\eta-2)^3} \\ &- \frac{2(27\eta^6 - 198\eta^5 + 502\eta^4 - 438\eta^3 - 53\eta^2 + 140\eta + 60)(\eta-1)\ln(1-\eta)}{9(\eta-2)^4} \\ &+ \frac{1}{54(\eta-2)^3}(-48\eta^6(\ln(2048)-6) + 5(32\pi^2 - 339)\eta^5 + (2622 - 960\pi^2)\eta^4 \\ &+ 15(77 + 128\pi^2)\eta^3 - 10(435 + 128\pi^2)\eta^2 + 612\eta + 72(19 + \ln(256))) \\ &+ \frac{5}{3}(2\eta+1)(\eta-1)^2\ln\left(\frac{m_b^2}{\mu^2}\right) - \frac{80}{9}\eta^2\mathrm{Li}_2\left(\frac{\eta-1}{\eta-2}\right) + \frac{80}{9}\eta^2\mathrm{Li}_2\left(\frac{2(\eta-1)}{\eta-2}\right) \\ &- \frac{160\eta^2\mathrm{Li}_2(\eta)}{9} - \frac{5}{9}(2\eta+1)(\eta-1)^2 X_R + \frac{5}{9}(2\eta+1)(\eta-1)^2 Y_R, \end{aligned} \tag{B17}$$

$$g_3[{}^3D_1^{[1]}] = -\frac{2}{135}(10\eta+1)(40\eta^2 - 64\eta + 1)\ln(\eta) + \frac{1}{405}(-4304\eta^3 + 5547\eta^2 + 300\eta - 1543) + \frac{80}{27}(2\eta+1)(\eta-1)^2\ln(1-\eta) - \frac{40}{27}(2\eta+1)(\eta-1)^2\ln\left(\frac{\mu_\Lambda^2}{4m_c^2}\right). \tag{B18}$$

For ${}^3D_2^{[1]}$,

$$g_1[{}^3D_2^{[1]}] = 0, \tag{B19}$$

$$g_2[{}^3D_2^{[1]}] = 0, \tag{B20}$$

$$g_3[{}^3D_2^{[1]}] = -\frac{4}{45}(214\eta^3 - 273\eta^2 - 30\eta + 89) - \frac{8}{15}(20\eta^3 - 30\eta^2 - 2\eta + 1)\ln(\eta) + \frac{16}{3}(2\eta+1)(\eta-1)^2\ln(1-\eta) - \frac{8}{3}(2\eta+1)(\eta-1)^2\ln\left(\frac{\mu_\Lambda^2}{4m_c^2}\right). \tag{B21}$$

For ${}^3D_3^{[1]}$,

$$g_1[{}^3D_3^{[1]}] = 0, \tag{B22}$$

$$g_2[{}^3D_3^{[1]}] = 0, \tag{B23}$$

$$g_3[{}^3D_3^{[1]}] = \frac{8}{315}(2\eta^3 - 11\eta^2 + 10\eta - 1) + \frac{16}{315}(4\eta-1)\ln(\eta). \tag{B24}$$

[1] N. Brambilla, S. Eidelman, B. K. Heltsley, R. Vogt, G. T. Bodwin, E. Eichten, A. D. Frawley, A. B. Meyer *et al.*, Heavy quarkonium: Progress, puzzles, and opportunities, Eur. Phys. J. C **71**, 1534 (2011).

[2] N. Brambilla, S. Eidelman, P. Foka, S. Gardner, A. S. Kronfeld, M. G. Alford, R. Alkofer, M. Butenschoen *et al.*, QCD and strongly coupled gauge theories: Challenges and perspectives, Eur. Phys. J. C **74**, 2981 (2014).

[3] S. L. Olsen, A new hadron spectroscopy, Front. Phys. China **10**, 121 (2015).

[4] V. Bhardwaj *et al.* (Belle Collaboration), Evidence of a New Narrow Resonance Decaying to $\chi_{c1}\gamma$ in $B \to \chi_{c1}\gamma K$, Phys. Rev. Lett. **111**, 032001 (2013).

[5] P. Pakhlov *et al.* (Belle Collaboration), Production of New Charmoniumlike States in $e^+e^- \to J/\psi D^* \bar{D}^*$ at $\sqrt{s} \sim 10.6$ GeV, Phys. Rev. Lett. **100**, 202001 (2008).

[6] Z. G. He, Y. Fan, and K. T. Chao, NRQCD predictions of D-wave quarkonia $^3D_J (J = 1, 2, 3)$ decay into light hadrons at order α_S^3, Phys. Rev. D **81**, 074032 (2010).

[7] B. Q. Li and K. T. Chao, Higher charmonia and X, Y, Z states with screened potential, Phys. Rev. D **79**, 094004 (2009).

[8] K. A. Olive *et al.* (Particle Data Group Collaboration), Review of particle physics, Chin. Phys. C **38**, 090001 (2014).

[9] Y. J. Gao, C. Meng, and K. T. Chao, $\psi(3770)$ and B meson exclusive decay $B \to \psi(3770)K$ in QCD factorization, Eur. Phys. J. A **28**, 361 (2006).

[10] Z. Z. Song, C. Meng, Y. J. Gao, and K. T. Chao, Infrared divergences of B meson exclusive decays to P wave charmonia in QCD factorization and nonrelativistic QCD, Phys. Rev. D **69**, 054009 (2004).

[11] G. T. Bodwin, E. Braaten, and G. P. Lepage, Rigorous QCD analysis of inclusive annihilation and production of heavy quarkonium, Phys. Rev. D **51**, 1125 (1995); **55**, 5853(E) (1997).

[12] F. Yuan, C. F. Qiao, and K. T. Chao, D wave charmonium production in B decays, Phys. Rev. D **56**, 329 (1997).

[13] P.w. Ko, J. Lee, and H. S. Song, Color octet mechanism in the inclusive D wave charmonium productions in B decays, Phys. Lett. B **395**, 107 (1997).

[14] M. Beneke, F. Maltoni, and I. Z. Rothstein, QCD analysis of inclusive B decay into charmonium, Phys. Rev. D **59**, 054003 (1999).

[15] Y. Fan, J.-Z. Li, C. Meng, and K.-T. Chao, B-meson semi-inclusive decay to 2^{-+} charmonium in NRQCD and $X(3872)$, Phys. Rev. D **85**, 034032 (2012).

[16] G. Buchalla, A. J. Buras, and M. E. Lautenbacher, Weak decays beyond leading logarithms, Rev. Mod. Phys. **68**, 1125 (1996).

[17] H. Han, Y. Q. Ma, C. Meng, H. S. Shao, and K. T. Chao, η_c Production at LHC and Indications on the Understanding of J/ψ Production, Phys. Rev. Lett. **114**, 092005 (2015).

[18] M. Gremm and A. Kapustin, Annihilation of S-wave quarkonia and the measurement of α_s, Phys. Lett. B **407**, 323 (1997).

[19] Y. Fan, Z. G. He, Y. Q. Ma, and K. T. Chao, Predictions of light hadronic decays of heavy quarkonium $^1D_2$ states in nonrelativistic QCD, Phys. Rev. D **80**, 014001 (2009).

[20] Y. Fan, Estimate of the h_c decay width in NRQCD, Topical Seminar on Frontier of Particle Physics 2010: Charm and Charmonium Physics, Beijing, China, 2010, http://indico.ihep.ac.cn/conferenceTimeTable.py?confId=1484 (unpublished).

[21] E. J. Eichten and C. Quigg, Quarkonium wave functions at the origin, Phys. Rev. D **52**, 1726 (1995).

[22] A. J. Buras and P. H. Weisz, QCD nonleading corrections to weak decays in dimensional regularization and 't Hooft–Veltman schemes, Nucl. Phys. **B333**, 66 (1990).

[23] Y.-P. Kuang and T.-M. Yan, Hadronic transitions of D wave quarkonium and $\psi(3770) \to J/\psi\pi\pi$, Phys. Rev. D **41**, 155 (1990).

[24] Y.-B. Ding, D.-H. Qin, and K.-T. Chao, Electric dipole transitions of $\psi(3770)$ and S-D mixing between $\psi(3686)$ and $\psi(3770)$, Phys. Rev. D **44**, 3562 (1991).

[25] J. L. Rosner, Charmless final states and S- and D-wave mixing in the ψ'', Phys. Rev. D **64**, 094002 (2001).

[26] T. Barnes, S. Godfrey, and E. S. Swanson, Higher charmonia, Phys. Rev. D **72**, 054026 (2005).